ARTICLE

doi:10.1038/nature10915

Global warming preceded by increasing carbon dioxide concentrations during the last deglaciation

Jeremy D. Shakun[1,2], Peter U. Clark[3], Feng He[4], Shaun A. Marcott[3], Alan C. Mix[3], Zhengyu Liu[4,5,6], Bette Otto-Bliesner[7], Andreas Schmittner[3] & Edouard Bard[8]

The covariation of carbon dioxide (CO_2) concentration and temperature in Antarctic ice-core records suggests a close link between CO_2 and climate during the Pleistocene ice ages. The role and relative importance of CO_2 in producing these climate changes remains unclear, however, in part because the ice-core deuterium record reflects local rather than global temperature. Here we construct a record of global surface temperature from 80 proxy records and show that temperature is correlated with and generally lags CO_2 during the last (that is, the most recent) deglaciation. Differences between the respective temperature changes of the Northern Hemisphere and Southern Hemisphere parallel variations in the strength of the Atlantic meridional overturning circulation recorded in marine sediments. These observations, together with transient global climate model simulations, support the conclusion that an antiphased hemispheric temperature response to ocean circulation changes superimposed on globally in-phase warming driven by increasing CO_2 concentrations is an explanation for much of the temperature change at the end of the most recent ice age.

Understanding the causes of the Pleistocene ice ages has been a significant question in climate dynamics since they were discovered in the mid-nineteenth century. The identification of orbital frequencies in the marine $^{18}O/^{16}O$ record, a proxy for global ice volume, in the 1970s demonstrated that glacial cycles are ultimately paced by astronomical forcing[1]. Initial measurements of air bubbles in Antarctic ice cores in the 1980s revealed that greenhouse gas concentrations also increased and decreased over the last glacial cycle[2,3], suggesting they too may be part of the explanation. The ice-core record now extends back 800,000 yr and shows that local Antarctic temperature was strongly correlated with and seems to have slightly led changes in CO_2 concentration[4]. The implication of this relationship for understanding the role of CO_2 in glacial cycles, however, remains unclear. For instance, proxy data have variously been interpreted to suggest that CO_2 was the primary driver of the ice ages[5], a more modest feedback on warming[6,7] or, perhaps, largely a consequence rather than cause of past climate change[8]. Similarly, although climate models generally require greenhouse gases to explain globalization of the ice-age signal, they predict a wide range (one-third to two-thirds) in the contribution of greenhouse gases to ice-age cooling, with additional contributions from ice albedo and other effects[9,10]. Moreover, models have generally used prescribed forcings to simulate snapshots in time and thus by design do not distinguish the timing of changes in various forcings relative to responses.

Global temperature reconstructions and transient model simulations spanning the past century and millennium have been essential to the attribution of recent climate change, and a similar strategy would probably improve our understanding of glacial cycle dynamics. Here we use a network of proxy temperature records that provide broad spatial coverage to show that global temperature closely tracked the increase in CO_2 concentration over the last deglaciation, and that variations in the Atlantic meridional overturning circulation (AMOC) caused a seesawing of heat between the hemispheres, supporting an early hypothesis that identified potentially important roles for these mechanisms[11]. These findings, supported by transient simulations with a coupled ocean–atmosphere general circulation model, can explain the lag of CO_2 behind Antarctic temperature in the ice-core record and are consistent with an important role for CO_2 in driving global climate change over glacial cycles.

Global temperature

We calculate the area-weighted mean of 80 globally distributed, high-resolution proxy temperature records to reconstruct global surface temperature during the last deglaciation (Methods and Fig. 1). The global temperature stack shows a two-step rise, with most warming occurring during and right after the Oldest Dryas and Younger Dryas intervals and relatively little temperature change during the Last Glacial Maximum (LGM), the Bølling–Allerød interval and the early Holocene epoch (Fig. 2a). The atmospheric CO_2 record from the EPICA Dome C ice core[12], which has recently been placed on a more accurate timescale[13], has a similar two-step structure and is strongly correlated with the temperature stack ($r^2 = 0.94$ (coefficient of determination), $P = 0.03$; Fig. 2a).

Lag correlations quantify the timing of change in the temperature stack relative to CO_2 from 20–10 kyr ago, an interval that spans the period during which low LGM CO_2 concentrations increased to almost pre-industrial values. Our results indicate that CO_2 probably leads global warming over the course of the deglaciation (Fig. 2b). A comparison of the global temperature stack with Antarctic temperature provides further support for this relative timing, in showing that

[1]Department of Earth and Planetary Sciences, Harvard University, Cambridge, Massachusetts 02138, USA. [2]Lamont-Doherty Earth Observatory, Columbia University, Palisades, New York 10964, USA. [3]College of Earth, Ocean, and Atmospheric Sciences, Oregon State University, Corvallis, Oregon 97331, USA. [4]Center for Climatic Research, University of Wisconsin, Madison, Wisconsin 53706, USA. [5]Department of Atmospheric and Oceanic Sciences, University of Wisconsin, Madison, Wisconsin 53706, USA. [6]Laboratory for Ocean-Atmosphere Studies, Peking University, Beijing 100871, China. [7]Climate and Global Dynamics Division, National Center for Atmospheric Research, Boulder, Colorado 80307-3000, USA. [8]CEREGE, Collège de France, CNRS-Université Aix-Marseille, Europole de l'Arbois, 13545 Aix-en-Provence, France.

©2012 Macmillan Publishers Limited. All rights reserved

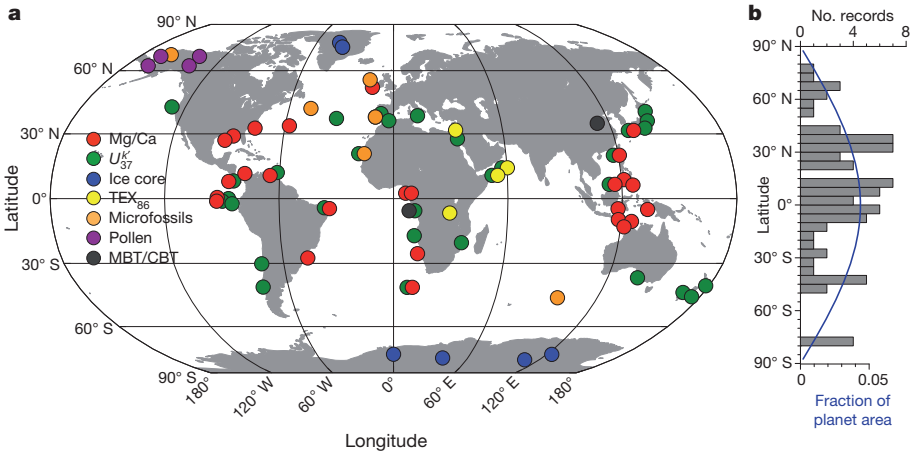

Figure 1 | Proxy temperature records. **a**, Location map. CBT, cyclization ratio of branched tetraethers; MBT, methylation index of branched tetraethers; TEX_{86}, tetraether index of tetraethers consisting of 86 carbon atoms; $U^{K'}_{37}$, alkenone unsaturation index. **b**, Distribution of the records by latitude (grey histogram) and areal fraction of the planet in 5° steps (blue line).

although the structure of the global stack is similar to the pattern of Antarctic temperature change, it lags Antarctica by several centuries to a millennium throughout most of the deglaciation (Fig. 2a). Thus, the small apparent lead of Antarctic temperature over CO_2 in the ice-core records[12,14] does not apply to global temperature. An additional evaluation of this result comes from an objective identification of inflection points in the CO_2 and global temperature records, which suggests that changes in CO_2 concentration were either synchronous with or led global warming during the various steps of the deglaciation (Supplementary Table 2). An important exception is the onset of deglaciation, which features about 0.3 °C of global warming before the initial increase in CO_2 ~17.5 kyr ago. This finding suggests that CO_2 was not the cause of initial warming. We return to this point below. Nevertheless, the overall correlation and phasing of global temperature and CO_2 are consistent with CO_2 being an important driver of global warming during the deglaciation, with the centennial-scale lag of temperature behind CO_2 being consistent with the thermal inertia of the climate system owing to ocean heat uptake and ice melting[15].

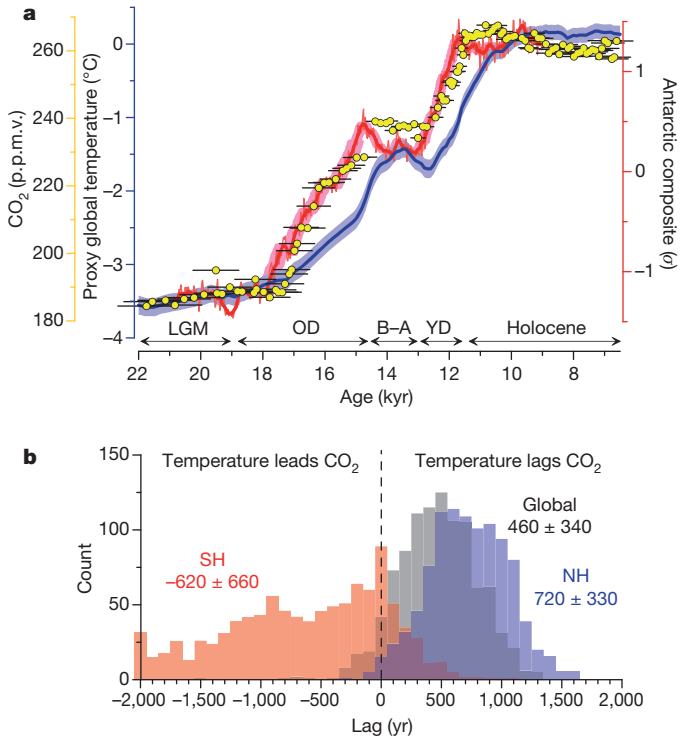

Figure 2 | CO_2 concentration and temperature. **a**, The global proxy temperature stack (blue) as deviations from the early Holocene (11.5–6.5 kyr ago) mean, an Antarctic ice-core composite temperature record[42] (red), and atmospheric CO_2 concentration (refs 12, 13; yellow dots). The Holocene, Younger Dryas (YD), Bølling–Allerød (B–A), Oldest Dryas (OD) and Last Glacial Maximum (LGM) intervals are indicated. Error bars, 1σ (Methods); p.p.m.v., parts per million by volume. **b**, The phasing of CO_2 concentration and temperature for the global (grey), Northern Hemisphere (NH; blue) and Southern Hemisphere (SH; red) proxy stacks based on lag correlations from 20–10 kyr ago in 1,000 Monte Carlo simulations (Methods). The mean and 1σ of the histograms are given. CO_2 concentration leads the global temperature stack in 90% of the simulations and lags it in 6%.

Although other mechanisms contributed to climate change during the ice ages, climate models suggest that their impacts were regional and thus cannot explain the global extent of temperature changes documented by our stacked record alone[9,16,17]. This conclusion is supported by the distinct differences, relative to the temperature stack, in the temporal variabilities of other likely climate change agents (Fig. 3). For example, insolation is a smoothly varying sinusoid that is in antiphase between the hemispheres and sums to near zero globally at the top of the atmosphere (Fig. 3f). Although spatial and temporal asymmetries in albedo could convert insolation to a non-zero forcing at Earth's surface, it is unlikely to account for much of the step-like structure and global nature of the temperature stack.

Similarly, although ice-sheet extent and its associated albedo (from ice cover and emergent continental shelves) and orographic forcing decreased through the deglaciation, global ice volume and area changed only slowly or not at all during intervals of pronounced global warming such as the Oldest Dryas and Younger Dryas, and the greatest volume or area loss in fact occurred during intervals of little or no warming around 19 kyr ago and the Bølling–Allerød (Fig. 3a, b). This distinction is particularly notable during the early Holocene, when the temperature stack had reached interglacial levels while nearly one-third of the excess global ice still remained, although we note that any ice-driven warming would have been partly offset by decreasing greenhouse gas forcing (Fig. 3c and Supplementary Fig. 29a). The apparently small influence of ice-sheet forcing on the temperature stack is consistent with general circulation models that suggest its effect was largely confined to the northern mid to high latitudes and was otherwise modest in the areas sampled by our proxy network[16–18], which is biased away from the ice sheets. Our results, therefore, do not preclude an important contribution to global mean warming from ice-sheet retreat, but suggest that much of this warming was spatially restricted and may be inherently under-represented owing to the lack of suitable palaeotemperature records from and proximal to areas formerly covered by ice.

©2012 Macmillan Publishers Limited. All rights reserved

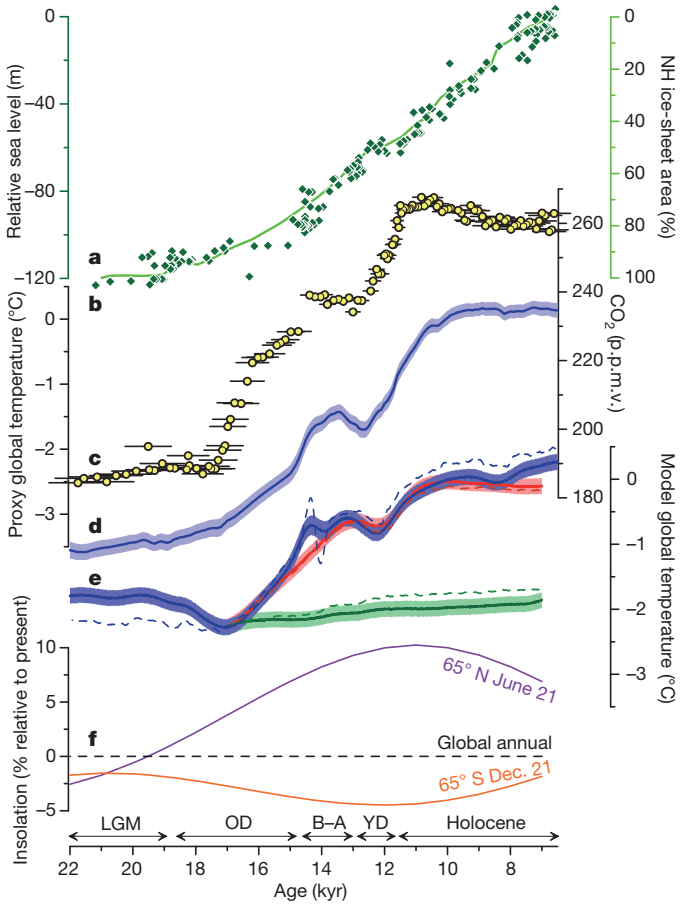

Figure 3 | Global temperature and climate forcings. **a**, Relative sea level[26] (diamonds). **b**, Northern Hemisphere ice-sheet area (line) derived from summing the extents of the Laurentide[43], Cordilleran[43] and Scandinavian (R. Gyllencreutz and J. Mangerud, personal communication) ice sheets through time. **c**, Atmospheric CO_2 concentration. **d**, Global proxy temperature stack. **e**, Modelled global temperature stacks from the ALL (blue), CO2 (red) and ORB (green) simulations. Dashed lines show global mean temperatures in the simulations, using sea surface temperatures over ocean and surface air temperatures over land. **f**, Insolation forcing for latitudes 65° N (purple) and 65° S (orange) at the local summer solstice, and global mean annual insolation (dashed black)[44]. Error bars, 1σ.

Unlike these regional-scale forcings, methane, nitrous oxide and possibly dust are global in nature. Because greenhouse gas forcing was dominated by CO_2 (ref. 19; Supplementary Fig. 29a), and because at the onsets of the Bølling–Allerød, Younger Dryas and Holocene the methane and nitrous oxide records have small step changes like those of the global temperature stack, including these greenhouse gases leaves the correlation with the stack essentially unchanged ($r^2 = 0.93$) and slightly decreases the temperature lag (250 ± 340 yr) (Supplementary Fig. 29). Global dust forcing is poorly constrained[19], however, and we cannot dismiss it as a potentially important driver of global temperature independent of greenhouse warming. Vegetation forcing is likewise difficult to assess[19] and may have significantly contributed to global warming. These uncertainties notwithstanding, we suggest that the increase in CO_2 concentration before that of global temperature is consistent with CO_2 acting as a primary driver of global warming, although its continuing increase is presumably a feedback from changes in other aspects of the climate system.

The global temperature lag behind CO_2 identified here relies critically on the chronological accuracy of these records. The largest uncertainty in the proxy age models is associated with radiocarbon reservoir corrections, which affect marine, but generally not terrestrial, records. A recent synthesis found similar temperature variabilities in land and ocean proxy records during the last deglaciation, but that the timing may be slightly earlier in the marine records[20] (Supplementary Fig. 4). Likewise, the pattern of temperature changes at upwelling sites, where reservoir ages may be more variable, is similar to that at non-upwelling sites but again seems somewhat older (Supplementary Fig. 4). These relationships imply that marine reservoir corrections may have been underestimated, which would shift the temperature stack to later times in some intervals and increase its average lag relative to CO_2. We also evaluated the EPICA Dome C CO_2 chronology[13] by comparing the Dome C methane record on this timescale with the more precisely dated Greenland composite methane record on the GICC05 timescale[21]. This comparison suggests that the EPICA Dome C CO_2 age model may be one to two centuries too young during parts of the deglaciation (Supplementary Fig. 7), which would further increase the lead of CO_2 over global temperature. We thus regard the lag of global temperature behind CO_2 reported here as conservative.

Hemispheric temperatures

The lead of Antarctic temperature over global temperature indicates spatial variability in the pattern of deglacial warming. To examine this spatial variability further, we calculated separate temperature stacks for the Northern Hemisphere and Southern Hemisphere and found that the magnitude of deglacial warming in the two hemispheric stacks is nearly identical (Fig. 4b). Given that greater LGM cooling probably occurred in the areas affected by the Northern Hemisphere ice sheets[9,17], this result provides additional support for our inference that the proxy network under-represents the regional impact of the ice sheets. Each hemispheric stack also shows a two-step warming as seen in the global stack and the CO_2 record (Fig. 4a). Otherwise, the hemispheric stacks differ in two main ways. First, lag correlations suggest that whereas Southern Hemisphere temperature probably leads CO_2, consistent with the Antarctic ice-core results[12], Northern Hemisphere temperature lags CO_2 (Fig. 2b). Second, the Northern Hemisphere shows modest coolings coincident with the onset of Southern Hemisphere warmings, and the warming steps are concave-up in the north but are concave-down in the south (Fig. 4b).

Calculating the temperature difference, ΔT, between the two hemispheric stacks yields an estimate of the heat distribution between the hemispheres, and reveals two large millennial-scale oscillations that are one-quarter to one-third of the glacial–interglacial range in global temperature (Fig. 4d). We attribute the variability in ΔT to variations in the strength of the AMOC and its attendant effects on cross-equatorial heat transport[22,23]. A strong correlation of ΔT with a kinematic proxy (Pa/Th, the protactinium/thorium ratio) for the strength of the AMOC[24] ($r^2 = 0.79$, $P = 0.03$) supports this interpretation (Fig. 4g). We find that ΔT decreases during the Oldest Dryas and Younger Dryas intervals, when the Pa/Th record suggests that the AMOC is weak and heat transfer between the hemispheres is reduced, and that ΔT increases during the LGM, the Bølling–Allerød and the Holocene, when the AMOC is stronger and transports heat from the south to the north. Recalculating ΔT for Atlantic-only records yields the same relations, but they are more pronounced and better correlated with Pa/Th ($r^2 = 0.86$, $P = 0.01$), as would be expected given the importance of the AMOC in this ocean (Fig. 4d). We note that this seesawing of heat between the hemispheres explains the contrast between the lead of Antarctic temperature over CO_2 and the lag of global (and Northern Hemisphere) temperature behind CO_2.

Transient modelling

We evaluate potential physical explanations for the correlations between temperature, CO_2 concentration and AMOC variability in three transient simulations of the last deglaciation using the Community Climate System Model version 3 (CCSM3; ref. 25) of the US National Center for Atmospheric Research. The first simulation (ALL) runs from 22 to 6.5 kyr ago and is driven by changes in greenhouse gases, insolation, ice sheets and freshwater fluxes (the last of which is adjusted iteratively

©2012 Macmillan Publishers Limited. All rights reserved

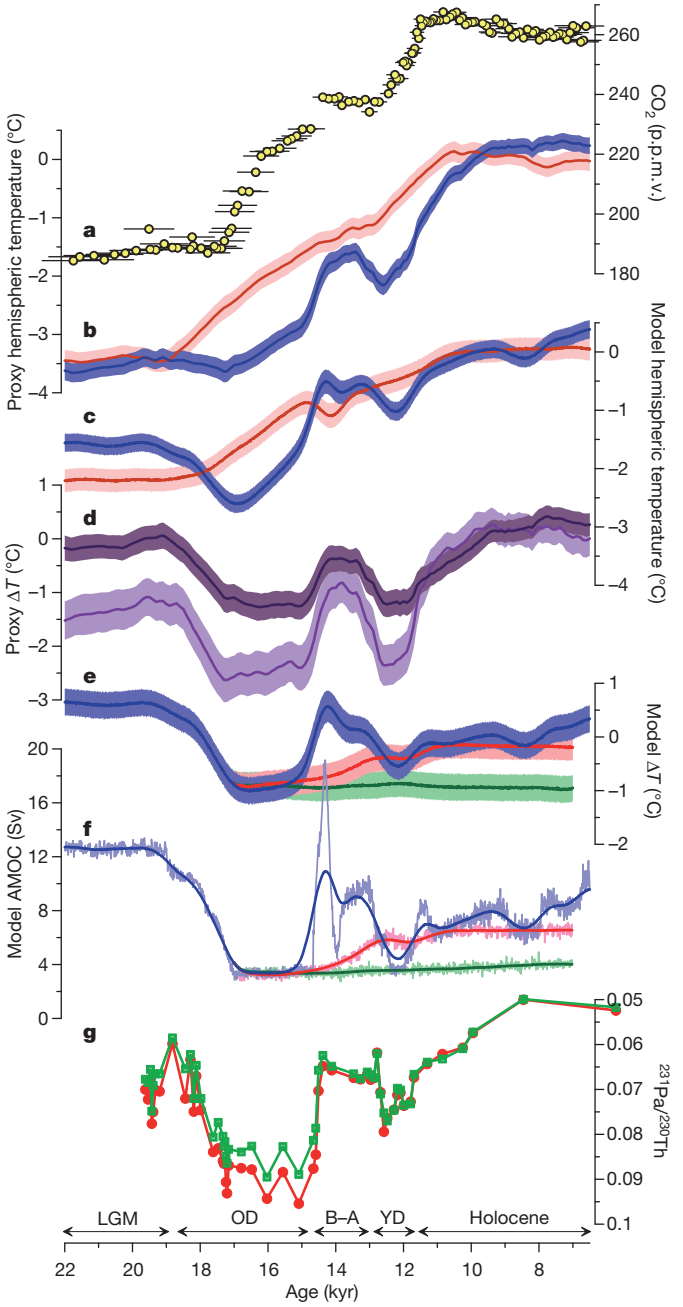

Figure 4 | Hemispheric temperatures. **a**, Atmospheric CO_2 concentration. **b**, Northern Hemisphere (blue) and Southern Hemisphere (red) proxy temperature stacks. **c**, Modelled Northern Hemisphere (blue) and Southern Hemisphere (red) temperature stacks from the ALL simulation. **d**, Northern Hemisphere minus Southern Hemisphere proxy temperature stacks (dark purple). North Atlantic minus South Atlantic region proxy temperature stacks (light purple). **e**, Modelled Northern Hemisphere minus Southern Hemisphere temperature stacks in the ALL (blue), CO2 (red) and ORB (green) simulations. **f**, Modelled AMOC strength in the ALL (blue), CO2 (red) and ORB (green) simulations. **g**, North Atlantic sediment core OCE326-GGC5 $^{231}Pa/^{230}Th$ (ref. 24). Temperatures are given as deviations from the early Holocene (11.5–6.5 kyr ago) mean. Error bars, 1σ.

and thus is a tunable parameter). The second simulation (CO2) is forced only by imposed changes in greenhouse gases (CO_2, methane and nitrous oxide), and the third simulation (ORB) is forced only by orbitally driven insolation variations. All other forcing factors for the second and third simulations, which run from 17 to 7 kyr ago, are held constant at their values at 17 kyr ago. All three simulations include dynamic vegetation feedback and a fixed annual cycle of aerosol forcing. We sample the model output at the locations of the 80 proxy records, recording sea surface temperatures for the marine records and surface air temperatures for the land records, and stacking these sampled model time series just as we did the data. We also correct sea surface temperature time series from the ALL simulation for sea-level changes by scaling the eustatic sea-level curve[26] to a warming by 0.32 °C at the LGM lowstand[27]. To simulate uncertainties in the model results comparable to those of the data, we generated 1,000 Monte Carlo simulations in which the modelled time series were perturbed with random age-model (±300 yr, 1σ) and temperature (±1 °C, 1σ) errors at each site.

The ALL model temperature stack from the 80 sites is similar to the global mean temperature from the model ($r^2 = 0.97$), suggesting that the proxy sites represent the globe fairly well, although the amplitude of warming is slightly smaller in the stack (Fig. 3e and Supplementary Fig. 12). The ALL model stack is also similar to the CO2 model stack in shape and amplitude ($r^2 = 0.98$; Fig. 3e). Because the CO2 model stack reflects a response to only greenhouse gas forcing, its similarity to the ALL stack suggests that greenhouse gases can explain most of the mean warming at these 80 sites. The ORB model stack, by contrast, shows only minor warming, consistent with a modest role for orbital forcing in directly driving global temperature changes.

Calculating the difference in model temperature between the Northern Hemisphere and the Southern Hemisphere at the proxy sites in the three simulations yields ΔT time series that are strongly correlated with variations in modelled AMOC strength in each simulation ($r^2 = 0.95$ for ALL, 0.98 for CO2; Fig. 4f). Only ΔT for the ALL simulation, however, shows millennial-scale variability similar to that seen in the proxy ΔT time series and the Pa/Th record (Fig. 4d, e, g). These results suggest that ocean circulation changes driven primarily by freshwater flux, rather than by direct forcing from greenhouse gases or orbits, are plausible causes of the hemispheric differences in temperature change seen in the proxy records. Furthermore, in the ALL simulation the Southern Hemisphere temperature stack leads Northern Hemisphere (and global) temperature during the two deglacial warming steps (Fig. 4c), supporting our inference that AMOC-driven internal heat redistributions explain the Antarctic temperature lead and global temperature lag relative to CO_2. Lag correlations from 20–10 kyr ago suggest that the modelled global temperature lags CO_2 concentration by 120 yr, which is within the uncertainty range of the proxy-based lag.

The trigger for deglacial warming

The proxy database provides an opportunity to explore what triggers deglacial warming. Substantial temperature change at all latitudes (Fig. 5b), as well as a net global warming of about 0.3 °C (Fig. 2a), precedes the initial increase in CO_2 concentration at 17.5 kyr ago, suggesting that CO_2 did not initiate deglacial warming. This early global warming occurs in two phases: a gradual increase between 21.5 and 19 kyr ago followed by a somewhat steeper increase between 19 and 17.5 kyr ago (Fig. 2a). The first increase is associated with mean warming of the northern mid to high latitudes, most prominently in Greenland, as there is little change occurring elsewhere at this time (Fig. 5 and Supplementary Fig. 20). The second increase occurs during a pronounced interhemispheric seesaw event (Fig. 5), presumably related to a reduction in AMOC strength, as seen in the Pa/Th record and our modelling (Fig. 4f, g). Tropical and Southern Hemisphere warming seem to have more than offset northern extratropical cooling, however, perhaps as a result of an asymmetry in the response of feedbacks such as Southern Ocean sea ice or tropical water vapour, leading to the global mean response. Alternatively, this non-zero-sum response may reflect proxy biases, as tropical warming is not equally evident in all proxies (Supplementary Fig. 20). In any event, we suggest that these spatiotemporal patterns of temperature change are consistent with warming at northern mid to high latitudes, leading to a reduction in the AMOC at ~19 kyr ago, being the trigger for the

©2012 Macmillan Publishers Limited. All rights reserved

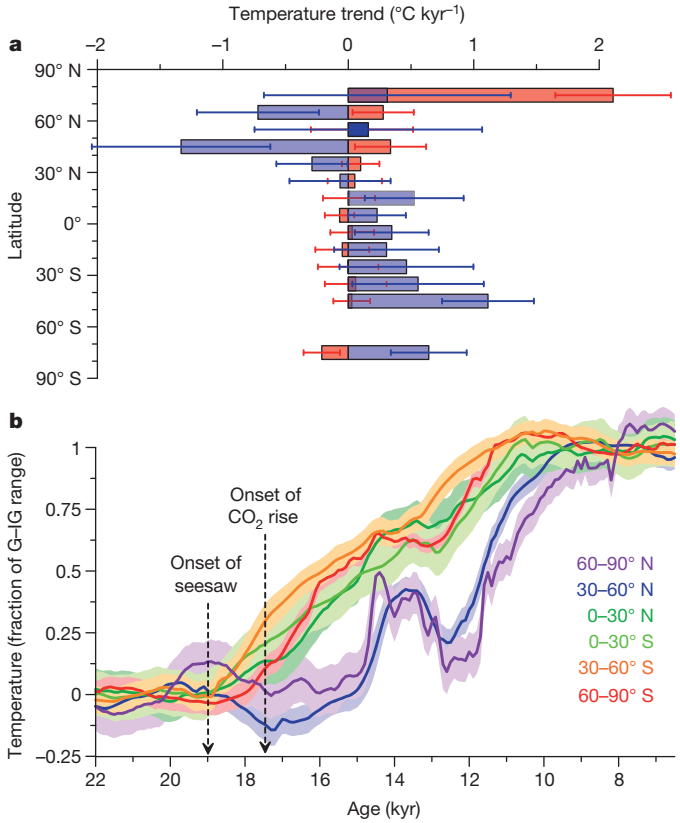

Figure 5 | Temperature change before increase in CO_2 concentration. **a**, Linear temperature trends in the proxy records from 21.5–19 kyr ago (red) and 19–17.5 kyr ago (blue) averaged in 10° latitude bins with 1σ uncertainties. **b**, Proxy temperature stacks for 30° latitude bands with 1σ uncertainties. The stacks have been normalized by the glacial–interglacial (G–IG) range in each time series to facilitate comparison.

global deglacial warming that followed, although more records will be required to confirm the extent and magnitude of early warming at such latitudes. A possible forcing model to explain this sequence of events starts with rising boreal summer insolation driving northern warming[28]. This leads to the observed retreat of Northern Hemisphere ice sheets[26] and the increase in sea level[29] commencing ~19 kyr ago (Fig. 3a, b), with the attendant freshwater forcing causing a reduction in the AMOC that warms the Southern Hemisphere through the bipolar seesaw[30].

Recent studies of the deglaciation[31,32] have shown a strong correlation between times of minima in the AMOC and maxima in CO_2 release, consistent with our ΔT proxy for AMOC strength (Fig. 4d), suggesting that a change in the AMOC may have also contributed to CO_2 degassing from the deep Southern Ocean though its influence on the extent of Southern Ocean sea ice[33], the position of the southern westerlies[34] or the efficiency of the biological pump[35]. Further insight into this relationship is provided by meridional differences in the timing of proxy temperature change following the reduction in AMOC after ~19 kyr ago. A near-synchronous seesaw response is seen from the high northern latitudes to the mid southern latitudes, whereas strong Antarctic warming and the increase in CO_2 concentration lag the AMOC change[36] (Figs 2a and 5b). This lag suggests that the high-southern-latitude temperature response to an AMOC perturbation may involve a time constant such as that from Southern Ocean thermal inertia[23,37], whereas the CO_2 response requires a threshold in AMOC reduction to displace southern winds or sea ice sufficiently[38] or to perturb the ocean's biological pump[35]. We also suggest that the delay of Antarctic warming that follows the AMOC seesaw event 19 kyr ago and occurs relative to the mid southern latitudes over the entire deglaciation (Fig. 5b) is difficult to reconcile with hypotheses invoking a southern high-latitude trigger for deglaciation[39,40].

Our global temperature stack and transient modelling point to CO_2 as a key mechanism of global warming during the last deglaciation. Furthermore, our results support an interhemispheric seesawing of heat related to AMOC variability and suggest that these internal heat redistributions explain the lead of Antarctic temperature over CO_2 while global temperature was in phase with or slightly lagged CO_2. Lastly, the global proxy database suggests that parts of the northern mid to high latitudes were the first to warm after the LGM, which could have initiated the reduction in the AMOC that may have ultimately caused the increase in CO_2 concentration.

METHODS SUMMARY

The data set compiled in this study contains most published high-resolution (median resolution, 200 yr), well-dated ($n = 636$ radiocarbon dates) temperature records from the last deglaciation (see Supplementary Information for the full database). Sixty-seven records are from the ocean and are interpreted to reflect sea surface temperatures, and the remaining 13 record air or lake temperatures on land. All records span 18–11 kyr ago and ~85% of them span 22–6.5 kyr ago. We recalibrated all radiocarbon dates with the IntCal04 calibration (Supplementary Information) and converted proxy units to temperature using the reservoir corrections and proxy calibrations suggested in the original publications. An exception to this was the alkenone records, which were recalibrated with a global core-top calibration[41]. The data were projected onto a $5° \times 5°$ grid, linearly interpolated to 100-yr resolution and combined as area-weighted averages. We used Monte Carlo simulations to quantify pooled uncertainties in the age models and proxy temperatures, although we do not account for analytical uncertainties or uncertainties related to lack of global coverage and spatial bias in the data set. In particular, the records are strongly biased towards ocean margins where high sedimentation rates facilitate the development of high-resolution records. Given these issues, we focus on the temporal evolution of temperature through the deglaciation rather than on its amplitude of change. The global temperature stack is not particularly sensitive to interpolation resolution, areal weighting, the number of proxy records, radiocarbon calibration, infilling of missing data or proxy type. Details on the experimental design of the transient model simulations can be found in ref. 25. The temperature stacks and proxy data set are available in Supplementary Information.

Full Methods and any associated references are available in the online version of the paper at www.nature.com/nature.

Received 16 September 2011; accepted 1 February 2012.

1. Hays, J. D., Imbrie, J. & Shackleton, N. J. Variations in the Earth's orbit: pacemaker of the ice ages. *Science* **194,** 1121–1132 (1976).
2. Delmas, R. J., Ascencio, J. M. & Legrand, M. Polar ice evidence that atmospheric CO_2 20,000 yr BP was 50% of present. *Nature* **284,** 155–157 (1980).
3. Neftel, A., Oeschger, H., Schwander, J., Stauffer, B. & Zumbrunn, R. Ice core sample measurements give atmospheric CO_2 content during the past 40,000 yr. *Nature* **295,** 220–223 (1982).
4. Lüthi, D. *et al.* High-resolution carbon dioxide concentration record 650,000–800,000 years before present. *Nature* **453,** 379–382 (2008).
5. Shackleton, N. J. The 100,000 year ice-age cycle identified and found to lag temperature, carbon dioxide and orbital eccentricity. *Science* **289,** 1897–1902 (2000).
6. Imbrie, J. *et al.* On the structure and origin of major glaciation cycles. 2. The 100,000-year cycle. *Paleoceanography* **8,** 699–735 (1993).
7. Alley, R. B. & Clark, P. U. The deglaciation of the northern hemisphere: a global perspective. *Annu. Rev. Earth Planet. Sci.* **27,** 149–182 (1999).
8. Toggweiler, J. R. & Lea, D. W. Temperature differences between the hemispheres and ice age climate variability. *Paleoceanography* **25,** PA2212 (2010).
9. Weaver, A. J., Eby, M., Fanning, A. F. & Wiebe, E. C. Simulated influence of carbon dioxide, orbital forcing and ice sheets on the climate of the Last Glacial Maximum. *Nature* **394,** 847–853 (1998).
10. Schneider von Deimling, T., Held, H., Ganopolski, A. & Rahmstorf, S. Climate sensitivity estimated from ensemble simulations of glacial climate. *Clim. Dyn.* **27,** 149–163 (2006).
11. Mix, A. C., Ruddiman, W. F. & McIntyre, A. Late Quaternary paleoceanography of the tropical Atlantic, 1: spatial variability of annual mean sea-surface temperatures, 0–20,000 years B.P. *Paleoceanography* **1,** 43–66 (1986).
12. Monnin, E. *et al.* Atmospheric CO_2 concentrations over the last glacial termination. *Science* **291,** 112–114 (2001).
13. Lemieux-Dudon, B. *et al.* Consistent dating for Antarctic and Greenland ice cores. *Quat. Sci. Rev.* **29,** 8–20 (2010).

©2012 Macmillan Publishers Limited. All rights reserved

14. Fischer, H., Wahlen, M., Smith, J., Mastroianni, D. & Deck, B. Ice core records of atmospheric CO_2 around the last three glacial terminations. *Science* **283,** 1712–1714 (1999).
15. Hansen, J. *et al.* Climate response times: dependence on climate sensitivity and ocean mixing. *Science* **229,** 857–859 (1985).
16. Manabe, S. & Broccoli, A. J. The influence of continental ice sheets on the climate of an ice age. *J. Geophys. Res.* **90,** 2167–2190 (1985).
17. Broccoli, A. J. Tropical cooling at the Last Glacial Maximum: an atmosphere-mixed layer ocean model simulation. *J. Clim.* **13,** 951–976 (2000).
18. Chiang, J. C. H. & Bitz, C. M. Influence of high latitude ice cover on the marine Intertropical Convergence Zone. *Clim. Dyn.* **25,** 477–496 (2005).
19. Jansen, E. *et al.* in *Climate Change 2007: The Physical Science Basis* (eds Solomon, S. *et al.*) 433–497 (Cambridge Univ. Press, 2007).
20. Clark, P. U. *et al.* Global climate evolution during the last deglaciation. *Proc. Natl Acad. Sci. USA* advance online publication doi:10.1073/pnas.1116619109 (13 February 2012).
21. Blunier, T. *et al.* Synchronization of ice core records via atmospheric gases. *Clim. Past* **3,** 325–330 (2007).
22. Crowley, T. J. North Atlantic Deep Water cools the Southern Hemisphere. *Paleoceanography* **7,** 489–497 (1992).
23. Stocker, T. F. & Johnsen, S. J. A minimum thermodynamic model for the bipolar seesaw. *Paleoceanography* **18,** 1087 (2003).
24. McManus, J. F., Francois, R., Gherardi, J.-M., Keigwin, L. D. & Brown-Leger, S. Collapse and rapid resumption of Atlantic meridional circulation linked to deglacial climate changes. *Nature* **428,** 834–837 (2004).
25. Liu, Z. *et al.* Transient simulation of last deglaciation with a new mechanism for Bølling-Allerød warming. *Science* **325,** 310–314 (2009).
26. Clark, P. U. *et al.* The Last Glacial Maximum. *Science* **325,** 710–714 (2009).
27. Schmittner, A. *et al.* Climate sensitivity estimated from temperature reconstructions of the Last Glacial Maximum. *Science* **334,** 1385–1388 (2011).
28. Alley, R. B., Brook, E. J. & Anandakrishnan, S. A northern lead in the orbital band: north-south phasing of Ice-Age events. *Quat. Sci. Rev.* **21,** 431–441 (2002).
29. Yokoyama, Y., Lambeck, K., De Deckker, P., Johnston, P. & Fifield, L. K. Timing of the Last Glacial Maximum from observed sea-level minima. *Nature* **406,** 713–716 (2000).
30. Clark, P. U., McCabe, A. M., Mix, A. C. & Weaver, A. J. Rapid rise of sea level 19,000 years ago and its global implications. *Science* **304,** 1141–1144 (2004).
31. Marchitto, T. M., Lehman, S. J., Ortiz, J. D., Fluckiger, J. & van Geen, A. Marine radiocarbon evidence for the mechanism of deglacial atmospheric CO_2 rise. *Science* **316,** 1456–1459 (2007).
32. Skinner, L. C., Fallon, S., Waelbroeck, C., Michel, E. & Barker, S. Ventilation of the deep Southern Ocean and deglacial CO_2 rise. *Science* **328,** 1147–1151 (2010).
33. Stephens, B. B. & Keeling, R. F. The influence of Antarctic sea ice on glacial-interglacial CO_2 variations. *Nature* **404,** 171–174 (2000).
34. Toggweiler, J. R., Russell, J. L. & Carson, S. R. Midlatitude westerlies, atmospheric CO2, and climate change during the ice ages. *Paleoceanography* **21,** PA2005 (2006).
35. Schmittner, A. & Galbraith, E. D. Glacial greenhouse-gas fluctuations controlled by ocean circulation changes. *Nature* **456,** 373–376 (2008).
36. Barker, S. *et al.* Interhemispheric Atlantic seesaw response during the last deglaciation. *Nature* **457,** 1097–1102 (2009).
37. Schmittner, A., Saenko, O. & Weaver, A. J. Coupling of the hemispheres in observations and simulations of glacial climate change. *Quat. Sci. Rev.* **22,** 659–671 (2003).
38. Anderson, R. F. *et al.* Wind-driven upwelling in the Southern Ocean and the deglacial rise in atmospheric CO_2. *Science* **323,** 1443–1448 (2009).
39. Stott, L., Timmermann, A. & Thunell, R. Southern hemisphere and deep-sea warming led deglacial atmospheric CO_2 rise and tropical warming. *Science* **318,** 435–438 (2007).
40. Huybers, P. & Denton, G. Antarctic temperature at orbital timescales controlled by local summer duration. *Nature Geosci.* **1,** 787–792 (2008).
41. Müller, P. J., Kirst, G., Ruhland, G., von Storch, I. & Rosell-Mele, A. Calibration of the alkenone paleotemperature index $U_{37}^{K'}$ based on core-tops from the eastern South Atlantic and the global ocean (60°N-60°S). *Geochim. Cosmochim. Acta* **62,** 1757–1772 (1998).
42. Pedro, J. B. *et al.* The last deglaciation: timing the bipolar seesaw. *Clim. Past Discuss.* **7,** 397–430 (2011).
43. Dyke, A. S. in *Quaternary Glaciations: Extent and Chronology* Vol. 2b (eds Ehlers, J. & Gibbard, P. L.) 373–424 (Elsevier, 2004).
44. Laskar, J. *et al.* A long term numerical solution for the insolation quantities of the Earth. *Astron. Astrophys.* **428,** 261–285 (2004).

Supplementary Information is linked to the online version of the paper at www.nature.com/nature.

Acknowledgements Discussions with numerous people, including E. J. Brook, A. E. Carlson, N. G. Pisias and J. Shaman, contributed to this research. We acknowledge the palaeoclimate community for generating the proxy data sets used here. In particular, we thank S. Barker, T. Barrows, E. Calvo, J. Kaiser, A. Koutavas, Y. Kubota, V. Peck, C. Pelejero, J.-R. Petit, J. Sachs, E. Schefuß, J. Tierney and G. Wei for providing proxy data, and R. Gyllencreutz and J. Mangerud for providing unpublished results of the DATED Project on the retreat history of the Eurasian ice sheets. The NOAA NGDC and PANGAEA databases were also essential to this work. This research used resources of the Oak Ridge Leadership Computing Facility, located in the National Center for Computational Sciences at Oak Ridge National Laboratory, which is supported by the Office of Science of the Department of Energy under contract no. DE-AC05-00OR22725. NCAR is sponsored by the NSF. J.D.S. is supported by a NOAA Climate and Global Change Postdoctoral Fellowship. This research was supported by the NSF Paleoclimate Program for the Paleovar Project through grant AGS-0602395.

Author Contributions J.D.S. designed the study, synthesized and analysed data, and wrote the manuscript with P.U.C. F.H., Z.L. and B.O.-B. did the transient modelling. S.A.M. and A.C.M. contributed to data analysis. A.S. helped interpret AMOC–CO_2 linkages. E.B. provided data and discussion on the radiocarbon calibration. All authors discussed the results and provided input on the manuscript.

Author Information Reprints and permissions information is available at www.nature.com/reprints. The authors declare no competing financial interests. Readers are welcome to comment on the online version of this article at www.nature.com/nature. Correspondence and requests for materials should be addressed to J.D.S. (shakun@fas.harvard.edu).

©2012 Macmillan Publishers Limited. All rights reserved

METHODS

Age control. All radiocarbon dates were recalibrated using Calib 6.0.1 with the IntCal04 calibration and the reservoir corrections suggested in the original publications. Age models based on tuning were left unchanged from the original publications. We used the GICC05 timescale for NGRIP and GRIP, the timescale of ref. 13 for EDML and Dome C, and glaciological age models for the Dome F and Vostok ice cores.

Proxy temperatures. We converted proxy units to temperature for all alkenone, Mg/Ca and TEX_{86} records using the calibrations suggested by the original authors for Mg/Ca and TEX_{86} and the global core-top calibration for alkenone records[41]. We used the published temperature reconstructions for Antarctic ice-core, pollen, microfossil assemblage and MBT/CBT records and the GISP2 borehole calibration for the Greenland ice cores[45]. Missing data values near the beginning and end of the ~15% of records not spanning the entire study interval were infilled using the method of regularized expectation maximization[46].

Stacking. The proxy data were projected onto a $5^\circ \times 5^\circ$ grid, linearly interpolated to 100-yr resolution and combined as area-weighted averages. We do not otherwise account for spatial biases in the dataset or lack of global coverage.

Uncertainty analysis. There are two main sources of uncertainty in the proxy records: age models and temperature calibration. We used a Monte Carlo approach to generate 1,000 realizations of each proxy temperature record after perturbing the records with chronological and temperature errors. These perturbed records were then averaged to yield 1,000 realizations of the global and hemispheric temperature stacks. The error bars on the temperature stacks represent the standard deviations of these 1,000 realizations, which provide an estimate of the propagated uncertainty due to uncertainties in the individual proxy records. A similar approach was applied to the transient model output to develop the modelled temperature stacks and error bars. We developed continuous uncertainty estimates for radiocarbon-based chronologies, taking into account radiocarbon date errors as well as interpolation uncertainty between dates using a random walk model[47]. Age-model uncertainties for tuned records, the Dome F and Vostok ice cores, and regional temperature reconstructions for Beringia[48] were assumed to be 2% (1σ). We used the Dome C and EDML ice-core age-model uncertainties[13] and GICC05 maximum counting errors[49,50] as 2σ uncertainties for the NGRIP and GRIP ice cores as suggested in ref. 50. We used the following 1σ temperature calibration uncertainties: alkenones, $T = (U^{K'}_{37} - 0.044 \pm 0.016)/(0.033 \pm 0.001)$ (ref. 41); Mg/Ca $= \pm 0.02B\exp(\pm 0.003AT)$, where A and B are constants (ref. 51); TEX_{86}, $\pm 1.7\,^\circ$C (ref. 52); ice cores, $\pm 10\%$ (ref. 53); pollen, microfossil assemblages and MBT/CBT, $\pm 1.5\,^\circ$C. We did not account for analytical uncertainties in proxy measurements. Chronological errors in the Monte Carlo simulations were temporally autocorrelated but were random in space (but this does not account for systematic errors among the proxy records due to uncertainties in the radiocarbon calibration), whereas temperature errors were assumed to be random in space and time. We note that our study is concerned with temperature anomalies and is thus sensitive to relative but not absolute temperature errors in a proxy record. See Supplementary Information for more details and examples. Age-model uncertainties for the Antarctic Dome C CO_2 record related to methane synchronization to Greenland were estimated on the basis of the combined uncertainties associated with Greenland layer counting, Greenland ice-age/gas-age differences and methane tuning to Antarctica. These uncertainties were used to generate 1,000 realizations of the CO_2 record, which together with the 1,000 temperature stack realizations yield the 1,000 temperature–concentration lead–lag estimates shown in Fig. 2b.

Robustness of results. We evaluated how well the proxy sites represent the globe by subsampling the twentieth-century instrumental temperature record and our transient modelling output of the deglaciation at the 80 proxy sites. Both approaches suggested that the mean of the proxy sites approximates the global mean fairly well. We recalculated the stack after interpolating the records to 500-yr resolution but this did not change the time series or its uncertainty. Differences in areal weighting affect the glacial–interglacial amplitude of the stack but have little impact on its structure. Jackknifing suggests that the stack is not particularly sensitive to the number of records used. A leave-one-out proxy jackknifing approach suggests that the correlation ($r^2 = 0.90$–0.95) and lead–lag relation (300–600-yr temperature lag) between global temperature and CO_2 concentration are not sensitive to proxy type. Statistical infilling of missing data values has negligible impact on the results. Although we here use the IntCal04 radiocarbon calibration, we tested the sensitivity of our results to this choice by recalibrating radiocarbon dates using the IntCal09 calibration. This makes the global stack up to 350 yr older during the Heinrich 1 interval, and shifts the overall phase lag relative to CO_2 concentration from 460 ± 340 to 350 ± 340 yr. We consider the IntCal04 calibration to be more accurate for the reasons discussed in Supplementary Information. Lag correlations suggest that Antarctic temperature led CO_2 concentration slightly throughout the deglaciation, whereas global temperature led CO_2 concentration at the onset of deglaciation but lagged behind it thereafter. The lead–lag relation between CO_2 concentration and the global temperature stack is not significantly changed by detrending the time series to remove the deglacial ramp in each quantity. The significance levels of the correlations between global temperature and CO_2 concentration and between Pa/Th and ΔT were determined by calculating effective sample sizes of these highly autocorrelated time series (CO_2 concentration, 4.3; global temperature, 4.1; Pa/Th, 5.4; ΔT, 6.2; Atlantic ΔT, 5.5) using equation 6.26 of ref. 54. See Supplementary Information for more discussion of these tests.

Model freshwater forcing. Whereas the forcing from insolation, greenhouse gases and ice sheets during the deglaciation are fairly well constrained, freshwater forcing is comparatively uncertain. Several model freshwater schemes were tested, and the final run was based on the meltwater scenario (Supplementary Fig. 30) that produced North Atlantic climate variability in best agreement with proxy reconstructions. The raw modelled AMOC time series (Fig. 4f, thin lines) were effectively smoothed with a Monte Carlo approach similar to the one used to develop the modelled temperature stacks (Fig. 4e), to facilitate direct comparison of the two. More specifically, the smoothed AMOC time series (Fig. 4f, bold lines) are the means of 1,000 realizations of the raw AMOC time series generated by perturbing them with 300-yr (1σ) age-model errors.

45. Cuffey, K. M. & Clow, G. D. Temperature, accumulation, and ice sheet elevation in central Greenland through the last deglacial transition. *J. Geophys. Res.* **102,** 26383–26396 (1997).
46. Schneider, T. Analysis of incomplete climate data: estimation of mean values and covariance matrices and imputation of missing values. *J. Clim.* **14,** 853–871 (2001).
47. Huybers, P. & Wunsch, C. A depth-derived Pleistocene age model: uncertainty estimates, sedimentation variability, and nonlinear climate change. *Paleoceanography* **19,** PA1028 (2004).
48. Viau, A. E., Gajewski, K., Sawada, M. C. & Bunbury, J. Low- and high-frequency climate variability in eastern Beringia during the past 25 000 years. *Can. J. Earth Sci.* **45,** 1435–1453 (2008).
49. Rasmussen, S. O. *et al.* Synchronization of the NGRIP, GRIP, and GISP2 ice cores across MIS 2 and palaeoclimatic implications. *Quat. Sci. Rev.* **27,** 18–28 (2008).
50. Svensson, A. *et al.* A 60000 year Greenland stratigraphic ice core chronology. *Clim. Past* **4,** 47–57 (2008).
51. Anand, P., Elderfield, H. & Conte, M. H. Calibration of Mg/Ca thermometry in planktonic foraminifera from a sediment trap time series. *Paleoceanography* **18,** 1050 (2003).
52. Kim, J. H., Schouten, S., Hopmans, E. C., Donner, B. & Damste, J. S. S. Global sediment core-top calibration of the TEX_{86} paleothermometer in the ocean. *Geochim. Cosmochim. Acta* **72,** 1154–1173 (2008).
53. Jouzel, J. *et al.* Magnitude of isotope/temperature scaling for interpretation of central Antarctic ice cores. *J. Geophys. Res.* **108,** 4361 (2003).
54. von Storch, H. & Zwiers, F. W. *Statistical Analysis in Climate Research* 115 (Cambridge Univ. Press, 1999).

©2012 Macmillan Publishers Limited. All rights reserved